

Investigation into the effects of inter-ply sliding during double diaphragm forming for multi-layered biaxial non-crimp fabrics

F. Yu, S. Chen, L.T. Harper^{*}, N.A. Warrior

Composites Research Group, University of Nottingham, Nottingham, UK

ARTICLE INFO

Keywords:

A. Fabrics/Textiles
A. Defects
C. Finite element analysis (FEA)
E. Forming

ABSTRACT

The effect of inter-ply sliding was investigated for multi-ply Non-Crimp Fabric (NCF) preforms during the Double Diaphragm Forming (DDF) process. A Finite Element (FE) model was employed to investigate the influence of the ply layout sequence and the coefficient of friction between fabric-fabric and fabric-diaphragm interfaces. Simulation results indicate that in-plane fibre compression, caused by dissimilar shear deformation between adjacent plies, can lead to out-of-plane wrinkles, where the wrinkle length is a function of the relative fibre angle at the ply-ply contact interface. The most severe wrinkles occurred when the inter-ply angle was 45° for a multi-ply biaxial NCF preform with a pillar stitch at 45° to the primary yarns. A second parametric study was conducted by incrementally reducing the coefficient of friction at the ply-ply interface. Experiments confirmed that out-of-plane wrinkles are sensitive to the friction resistance between NCF plies and therefore lubricating the fibres can minimise wrinkling defects caused by dissimilar inter-ply deformation.

1. Introduction

Fibre preforms for structural composite components are typically composed of multiple fabric plies, which are laid up following a specific ply orientation sequence to meet stiffness and strength requirements. Simultaneously forming multiple plies with different ply orientations over complex 3D shapes significantly increases the likelihood of defects compared to sequentially forming single plies, or forming multiple plies stacked at the same fibre orientation [1–3]. These forming induced defects, such as wrinkles and in-plane fibre buckling, can significantly reduce the mechanical performance of the final component [4–6], with the presence of fabric wrinkles reported to reduce the in-plane compressive strength in the loading direction by up to 40% [7]. Therefore understanding the cause of these defects and having the capability to predict their formation is critical for advancing the development of automated composite forming technologies.

Non-crimp fabrics (NCF) are typically composed of multiple layers of aligned straight yarns, bonded by through-thickness stitches. This type of fabric is of particular interest for manufacturing multi-ply preforms as it offers improved mechanical properties over woven fabrics due to the crimp-free architecture [8], is easier to handle due to higher in-plane shear resistance, and commonly has higher areal weights enabling faster material deposition. However, the asymmetric shear resistance

related to the stitch pattern [9] affects the inter-ply movement and hence influences the formation of defects.

Relative inter-ply movement between plies is the primary cause of wrinkles during the simultaneous forming of multiple fabric plies. When a thick fabric stack is formed over a male radius, such as a fillet edge on a tool, relative in-plane sliding between the plies is required to accommodate the “folding” of the ply stack [10,11], since each ply is required to deform by a different amount. Contacting plies at dissimilar orientations may compete against each other in terms of slippage direction or due to differing levels of inter-ply shear during the folding process. This results in in-plane fibre waviness and out-of-plane “rolling” of fibres due to bending-induced compression [12,13], which may eventually lead to wrinkles at the macro-scale. Similarly, a male punch used in press tool forming can locally constrain the inter-ply movement as it makes contact with the thick fabric stack, causing incompatible sliding between adjacent plies and consequently out-of-plane ply buckling in other areas of the preform [14]. This type of wrinkling mode was reported to be a function of the overall preform thickness, since more slippage has to be accommodated for thicker fabric stacks [11].

When forming stacked fabric plies of the same orientation, the relative motion between plies is negligible for thin layups, since each ply undergoes almost the same forming deformation [1,3]. However, plies stacked at different orientations tend to undergo different deformations

^{*} Corresponding author.

E-mail address: lee.harper@nottingham.ac.uk (L.T. Harper).

<https://doi.org/10.1016/j.compositesa.2021.106611>

Received 24 May 2021; Received in revised form 7 August 2021; Accepted 14 August 2021

Available online 20 August 2021

1359-835X/© 2021 The Authors. Published by Elsevier Ltd. This is an open access article under the CC BY license (<http://creativecommons.org/licenses/by/4.0/>).

Table 1
Material properties for FCIM359 biaxial NCF.

Fabric thickness	0.4 mm
Effective density	1200 kg/m ³
Effective modulus	3 GPa
Normalised fabric shear curve [9]	$P_{norm}^{NCF} = P_{norm}^{rotation} + P_{norm}^{stitch}$
$P_{norm}^{rotation}$	$(29.56\gamma_{12}^5 - 65.56\gamma_{12}^4 + 137.06\gamma_{12}^3 + 94.73\gamma_{12}^2 + 112.19\gamma_{12})$ N/m
P_{norm}^{stitch}	$\begin{cases} (2000\gamma_{12} - 120)\text{N/m}, & 0.06 \leq \gamma_{12} < 0.5 \\ (-3520\gamma_{12} + 2640)\text{N/m}, & 0.5 \leq \gamma_{12} < 0.75 \\ 0\text{N/m}, & \text{else} \end{cases}$
Bending moment–curvature curve [30]	$\begin{cases} M_{pos} = 0.19457 \cdot \kappa + 0.03139 \cdot \left(1 - \exp\left(-\frac{\kappa}{0.0040}\right)\right) \\ M_{neg} = 0.10279 \cdot \kappa + 0.03619 \cdot \left(1 - \exp\left(-\frac{\kappa}{0.0065}\right)\right) \end{cases}$ <p>M_{pos}, longitudinal fibres are on the tensile side. M_{neg}, longitudinal fibres are on the compressive side.</p>

Table 2
Material properties for FCIM359 [31].

Deformation mode	Expression
Uniaxial tension	$\sigma = 6.364 \times (e^{0.004451\epsilon} - e^{-0.07545\epsilon})$ MPa, $0 \leq \epsilon \leq 500\%$
Equibiaxial tension	$\sigma = 6.482 \times (e^{0.004871\epsilon} - e^{-0.12040\epsilon})$ MPa, $0 \leq \epsilon \leq 100\%$
Planar shear	$\sigma = 7.238 \times (e^{0.003774\epsilon} - e^{-0.08312\epsilon})$ MPa, $0 \leq \epsilon \leq 200\%$

Table 3
Coefficient of friction values used in forming simulations for contact interfaces with and without lubrication. $C_{fab-fab}^{fric}$, $C_{fab-dia}^{fric}$ are determined as the average value of friction coefficients at different fibre orientations for the corresponding surface pairing, according to the data shown in Fig. 2.

Interface pairing	Friction coefficient	
	Non-Lubricated	Lubricated
Fabric-fabric, $C_{fab-fab}^{fric}$	0.35	0.13
Fabric-diaphragm, $C_{fab-dia}^{fric}$	0.40	0.10
Diaphragm-tool, $C_{dia-tool}^{fric}$	0.25	–
Diaphragm-diaphragm, $C_{dia-dia}^{fric}$	0.32	0.08

in relation to the mould surface. This incompatible forming deformation and relative motion can generate frictional forces between adjacent plies, inducing either tensile or compressive stresses in the fibres. Excessive compressive force in the fibres can cause *meso*-scale defects, such as in-plane yarn buckling and laddering (gaps between tows in the transverse direction) [1,2]. This is typically observed in press tool forming, particularly when the motion of the yarns is restricted by contacting yarns from adjacent plies [1]. In contrast, in-plane fibre compression is typically observed in the form of local fabric wrinkles if the out-of-plane constraining force is insufficient, for example in Double Diaphragm Forming (DDF) where vacuum-only pressure is used to clamp the plies during forming [13,15–17].

Larger relative fibre angles between neighbouring plies can lead to more severe defects [2,18], due to the increase in inter-ply sliding at the interface. This is particularly common for quad-axial fibre layups (i.e. 0°, 90°, +45° and –45°), since the insertion of ± 45° fibres next to 0° or 90° fibres can cause in-plane compressive stresses along the principal fibre directions in each ply, as the in-plane fabric shear is restricted by

interfacial friction [3,16,19,20]. This mechanism was shown to be one of the dominant factors for wrinkle formation when forming quad-axial layups using a simple generic geometry with small curvatures [13,16,19,20]. One potential solution is to modify the layup sequence to use non-standard ply angles to facilitate compatible inter-ply deformation [19], whilst ensuring the overall composite stiffness is maintained.

Reducing the frictional resistance at ply contact interfaces can facilitate inter-ply sliding during forming, avoiding excessive in-plane-fabric compression. For example, prepreg resins exhibit a minimum viscosity within a certain elevated temperature window [21], therefore selecting an optimal processing temperature can lower the frictional forces at the ply interfaces, which has been demonstrated to be a potential way to control forming related defects [22–24]. However, controlling the resin viscosity and hence the inter-ply friction is not sufficient to overcome all wrinkles in multi-ply forming, particularly for quad-axial layups with low formability [19]. Reducing the sliding velocity has been demonstrated to reduce the dynamic coefficient of friction (CoF) for prepreps during material characterisation studies by up to 56% [25], with experimental studies using DDF demonstrating that reduced inter-ply friction can reduce wrinkling [26]. The use of thin polyester veils and phenoxy powder have been studied by Wang et al. [27] to improve inter-ply lubrication in DDF, where the maximum inter-ply frictional force was reduced by over 80% at room temperature when using the polyester veil. Experimental results demonstrated the capability of this lubrication method for mitigating wrinkles around the edge fillet of a generic aerospace spar geometry.

This paper investigates the forming behaviour of multiple bi-axial NCF plies during the double diaphragm forming process. A generic geometry is selected, which contains features that exhibit moderate variation in curvature along the length of the component, which enables the inter-ply movement between the NCF plies to be the dominant defect formation mechanism. A forming simulation tool that considers fabric bending behaviour [28,29] is employed to investigate the influence of ply layup sequence and interfacial frictional behaviour on the formation of out-of-plane wrinkles. The simulation tool is used to investigate the feasibility of using inter-ply lubrication to mitigate wrinkling for multi-ply NCF preforms.

2. Experiments

2.1. Materials

2.1.1. Non-crimp fabric

All layups in this study consisted of plies of NCF reinforcement (FCIM359), supplied by Hexcel, Leicester, UK. Each NCF ply consisted of two layers of non-crimp yarns in 24 K tow format stacked at ± 45°, assembled by pillar stitches at 0° in the roll direction. The NCF ply was 0.4 mm thick (uncompressed) with an areal mass of 440 g/m². The shear resistance and the bending behaviour of the NCF were characterised by the authors in previous studies [9,30], and the relevant data is reproduced in Table 1. The in-plane shear behaviour of the NCF is asymmetric for positive and negative shear deformation due to the pillar stitching pattern. The bending stiffness of the NCF decreases as the bending curvature increases, as a result of fibre slippage and tow buckling during bending. The NCF exhibits different bending resistance depending on the orientation of the yarns at the mesoscale, relative to the bending direction. Experiments were therefore performed by positioning the 0° fibres on both the upper surface and the lower surface about the mid-plane of the specimen. The parameters used for modelling the FCIM359

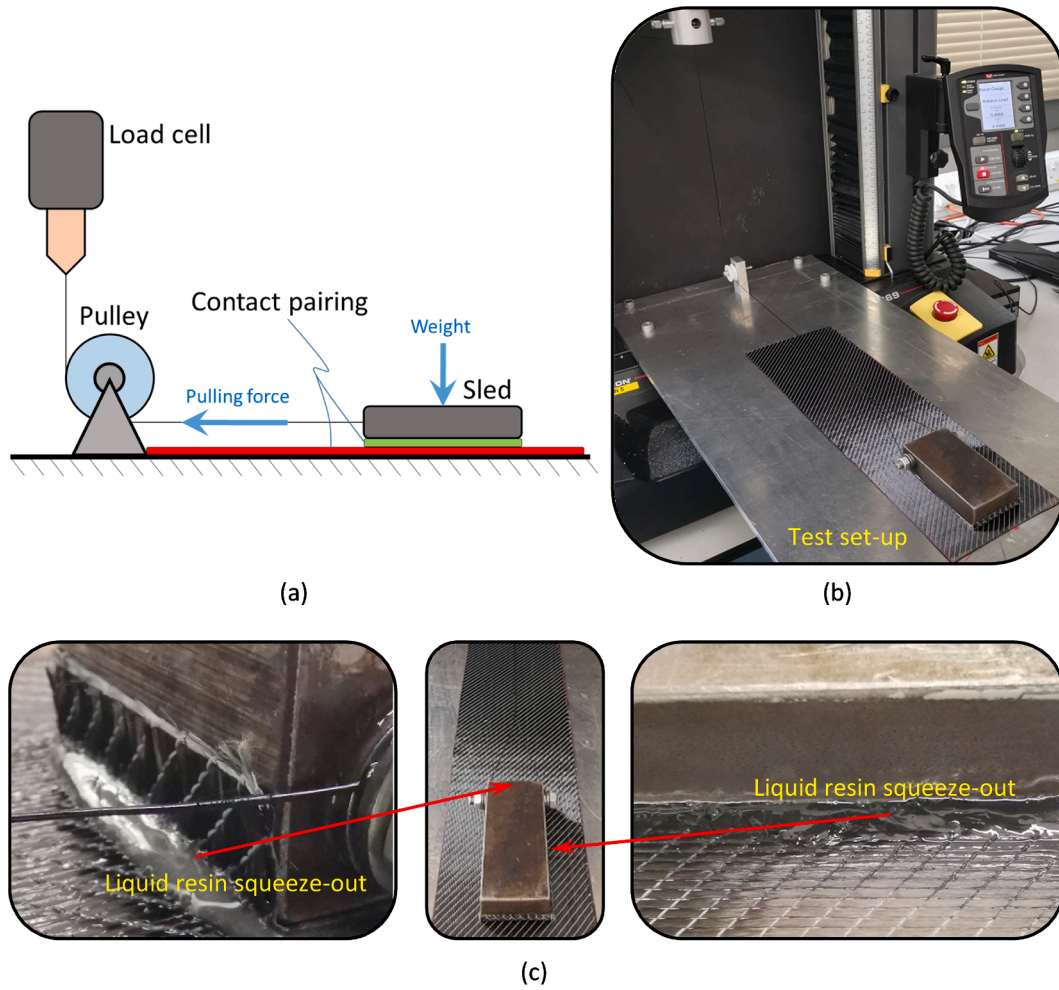


Fig. 1. (a) Schematic of the friction test and the surface condition of the specimens attached to the sled (b) Experimental set-up (c) Photographs showing liquid resin squeezing out beneath the sled during the test.

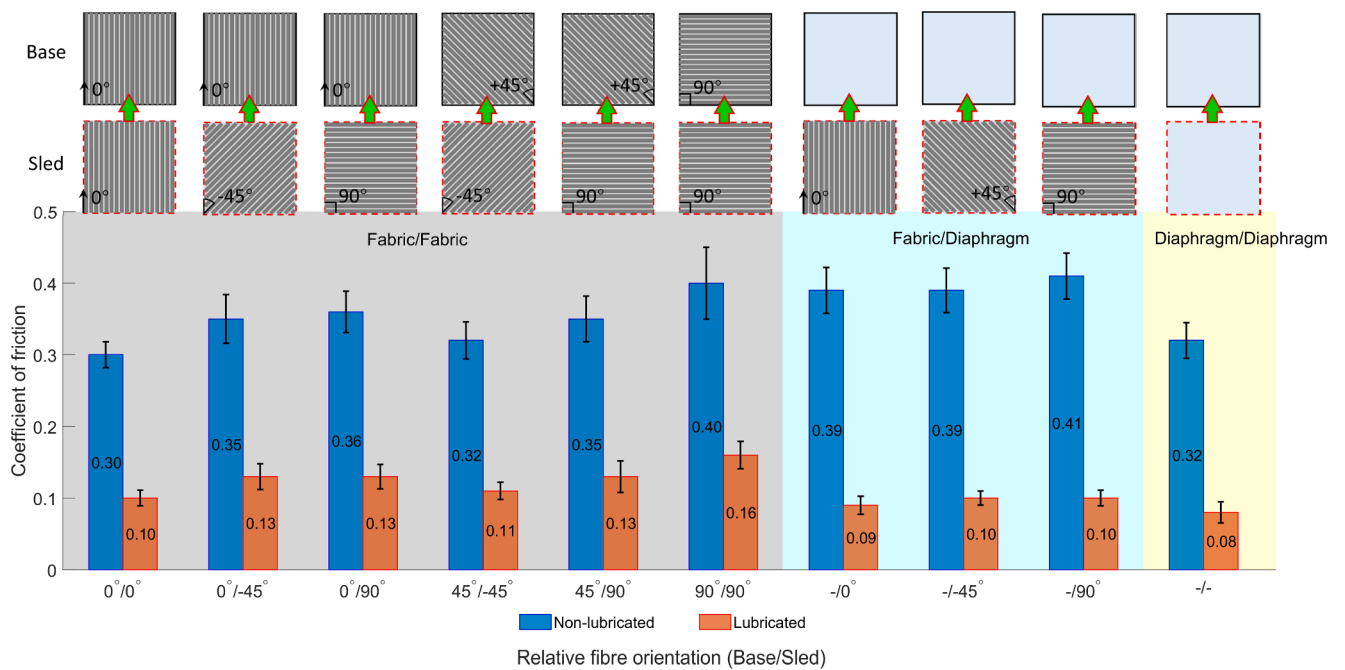


Fig. 2. Dynamic coefficient of friction for different material pairings, i.e. fabric-fabric (grey region), fabric-diaphragm (blue region) and diaphragm-diaphragm (yellow region), measured with and without liquid resin lubrication. Error bars denote the standard deviation from 5 experimental repeats.

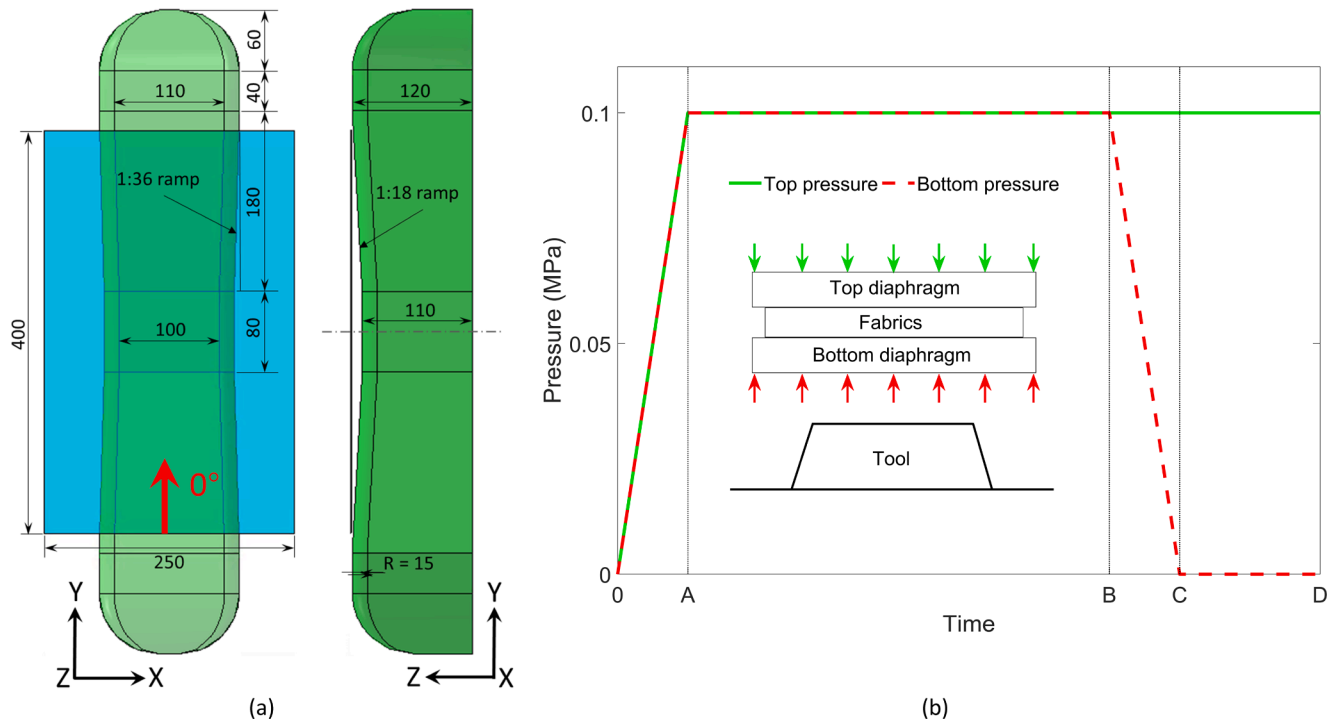


Fig. 3. (a) The dimensions of the tool geometry and fabric plies. (b) Graph indicating the pressure variation for the top and bottom diaphragms as a function of time. Inset image shows the fabric-diaphragm arrangement.

biaxial NCF material are presented in Table 1.

2.1.2. Diaphragm

A high elongation vacuum bag film, StretchLon HT-350 supplied by Tygavac Ltd UK, was used for the diaphragm material (strain to failure of $\sim 500\%$ under uniaxial tension [31]). The thickness of each diaphragm layer was measured to be 0.08 mm. The mechanical properties of the diaphragm material at ambient temperature were characterised by a series of tests, i.e. uniaxial tensile, equibiaxial tensile and planar shear tests. All tests were performed on a universal testing machine at a strain rate of 0.03 s^{-1} following the methodology presented by Chen et al. [29]. Three repeats were performed for each test to produce the mean stress-strain data for the corresponding deformation mode. The experimental data sets were fitted using an exponential relation with the root mean square error (RMSE) within 1.0 %, as listed in Table 2.

2.2. Coefficient of friction characterisation

Interfacial friction behaviour plays an important role in the formation of defects during multi-ply fabric forming [1,2], as areas of compression in the direction of the yarns can occur between contacting plies with dissimilar orientations. Reducing the inter-ply friction is therefore important to ensure that plies can slip more freely to avoid the formation of defects [3,27]. The use of a liquid resin was investigated during this study to lubricate the contact interfaces between all plies and the diaphragm films, in order to reduce the frictional resistance during DDF.

A sled test (ASTM D1894, ISO8295) was employed to characterise the frictional behaviour for different material contact pairings, including fabric-fabric, fabric-diaphragm, diaphragm-diaphragm and diaphragm-tool contacts, by measuring the relative movement between the sled

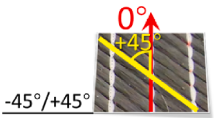
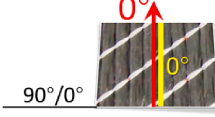
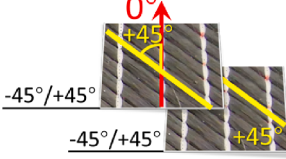
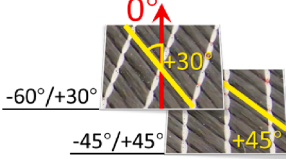
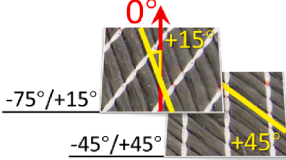
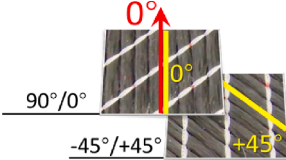
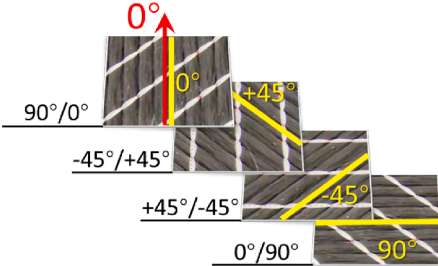
and the supporting plate. Friction tests were conducted for both dry surface pairings and lubricated surface pairings. The lubricated tests used a liquid epoxy resin (i.e. Prime™ 20LV, supplied by Gurit, UK). As shown in Fig. 1, material specimens in each contact pair were attached to the surface of the sled and the supporting plate using double-sided adhesive tape to represent the contact interaction in the forming process. The weight of the sled was used to calculate the applied normal force to the contact surface. The tangential force required to move the sled at a constant velocity across the supporting plate was recorded by a 1kN load cell connected to the crosshead of a universal testing machine (Instron 5581). All tests were carried out at ambient temperature (21°C).

The CoF was calculated from the ratio of the tangential (pulling) force and the normal force. For the lubricated surface pairings, the liquid resin was carefully applied on the surface of the base specimen ($300 \text{ mm} \times 125 \text{ mm}$) and then evenly distributed using a resin application roller to ensure the average areal weight of the liquid resin was 500 g/m^2 . Similarly, the liquid resin was evenly applied to the fabric ($125 \text{ mm} \times 50 \text{ mm}$) attached to the sled, with the same areal weight as the base specimen.

Six different fibre angle pairings were considered at the interface for the fabric-fabric contacts, $0^\circ/0^\circ$, $0^\circ/-45^\circ$, $0^\circ/90^\circ$, $+45^\circ/-45^\circ$, $+45^\circ/90^\circ$, $90^\circ/90^\circ$, as shown in Fig. 2. For the fabric-diaphragm contact, the diaphragm film was attached to the supporting plate and the fibre orientation of the fabric specimen on the sled was either 0° , 45° and 90° with respect to the sliding direction. Five test repeats were performed for each scenario and the average friction force versus sliding displacement curves are presented in Appendix A. The dynamic CoF for each test repeat was derived by taking an average of the dynamic CoFs between 100 mm and 200 mm in Figure A 1-Figure A 3. The mean values and the corresponding standard deviations for the CoF are presented in Fig. 2.

Table 4

Layup configurations for DDF trials. 0° direction (red arrow) is in line with the longitudinal direction of the tool in Fig. 3. The layup sequence is expressed from the lowermost side (closest to tool) to the uppermost side. For each biaxial NCF ply, the yellow line denotes the direction of the fibre tows on the upper side of the NCF ply, while the tows on the other side are perpendicular to the yellow line.

Layup	Layup schematic	Fibre orientation
M1		[-45°/ +45°]
M2		[90°/0°]
L1		[-45°/ +45°, -45°/ +45°]
L2		[-45°/ +45°, -60°/ +30°]
L3		[-45°/ +45°, -75°/ +15°]
L4		[-45°/ +45°, 90°/ 0°]
L5		[0°/90°, +45°/- 45°]s(i.e. [0°/90°, +45°/-45°, -45°/ +45°, 90°/ 0°])

It is understood that there are shortcomings for testing the lubricated fabric friction in this way, as resin is initially squeezed out at the interface, which affects the thickness of the lubricating layer and therefore the CoF, as demonstrated in Fig. 1(c). However, this method provides a qualitative assessment to support the simulation results. Relative to the dry fabric contact, the application of the liquid resin nominally reduces the CoF by 75% for the fabric-diaphragm contact

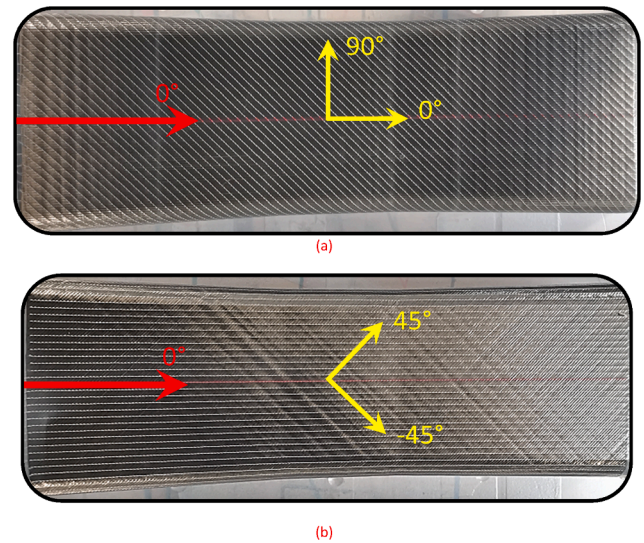


Fig. 4. Single ply NCF preforms produced by DDF. (a) [90°/0°] and (b) [-45°/+45°]. The red arrow denotes the longitudinal direction of the tool and the yellow arrow denotes the fibre direction prior to forming.

pairing, and approximately 63% for the fabric-fabric contact pairing. It was noted during the friction test that the liquid resin was squeezed out by the weight of the sled (see Fig. 1(c)), which is reflected in the force versus displacement curves in Appendix A (see Figure A 1-Figure A 3). The thickness of the lubricating layer (interfacial separation distance) is non-constant, which causes the pulling force to increase with increasing sliding distance. The effect of increasing the applied normal pressure and the resin viscosity on the inter-ply friction were not considered in this work.

2.3. Double diaphragm forming

A double diaphragm forming (DDF) machine developed at the University of Nottingham was used for the experimental forming trials [29]. Fabric plies were encapsulated by two layers of elastomer diaphragms and subsequently drawn over a male tool by a vacuum between the lower diaphragm and the machine bed. The tool was similar in shape to the ramped spar geometry used by Johnson et al. [19]. As shown in Fig. 3(a), recess features were assigned to both top and side faces of the spar, promoting some shear deformation to induce macro-scale defects. The tool was 640 mm in length and the in-plane dimension of the fabric plies was 400 mm × 250 mm. Since the ramp ratios of both the top and side surfaces of the tool were relatively small in magnitude (i.e. 1:18 for the top surface and 1:36 for the side surfaces), a small shear deformation ($\leq 10^\circ$) around the recessed region enabled the fabric plies to conform to the tool. Thus, the relative inter-ply movement dominated the formation of defects.

2.3.1. Multi-ply fabric forming

Forming experiments were performed using different multi-ply layups to investigate the formation of defects during DDF, along with single ply configurations formed for comparison. All layup configurations are listed in Table 4, where M1 and M2 are single ply cases and L1 – L5 are multi-ply cases. The red arrow in the schematic in Table 4 is in line with the longitudinal direction of the tool and the yellow line in each configuration denotes the direction of the fibre tows on the top side

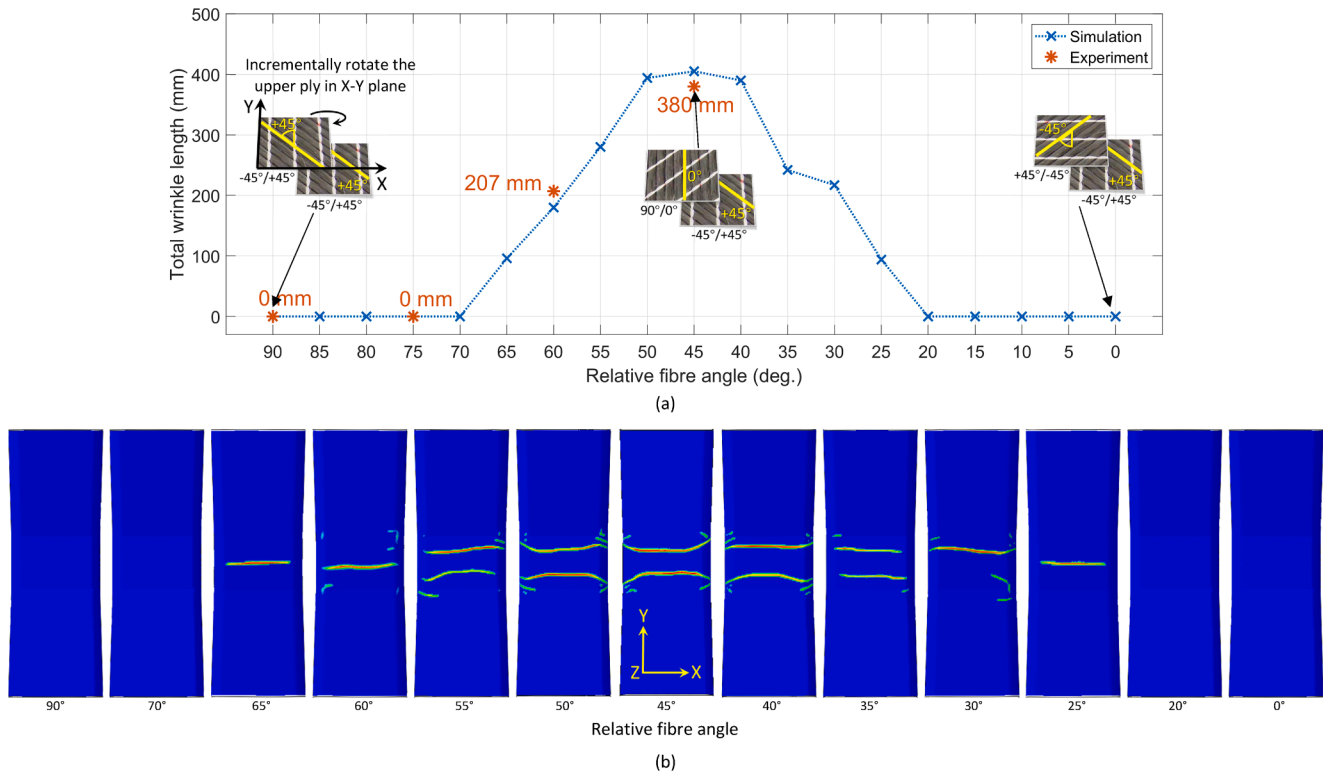


Fig. 5. (a) Length of wrinkles predicted from different layup orientations, compared with experimentally measured wrinkle lengths for the layups L1 - L4. (b) The wrinkle patterns predicted for different layup orientations.

of the ply. (The fibre direction on the reverse side of the ply is perpendicular to this yellow line).

As listed in Table 4, the fibre orientations for the single ply cases, M1 and M2, were $-45^\circ/+45^\circ$ and $90^\circ/0^\circ$ respectively. Layups L1-L4 in Table 4 consisted of two NCF plies, where the fibre orientation of the bottom ply (Ply 1) was fixed at $-45^\circ/+45^\circ$ and the uppermost ply (Ply 2) was prepared with different fibre orientations. At the contact interface between the adjacent plies, the relative difference in fibre orientation varied from 90° to 45° in increments of 15° . The layup L5 in Table 4 comprised four NCF plies laid up in a balanced symmetric sequence, i.e. $[0^\circ/90^\circ, +45^\circ/-45^\circ]_s$.

DDF experiments were initially performed for all configurations (M1, M2 and L1 - L5) using dry fabric plies. Experiments were then repeated for L4 and L5 using liquid resin applied to the surfaces of each fabric ply to investigate the effect of lubrication on the forming behaviour.

2.3.2. Defect visualisation

Structured White Light Scanning (SWLS) was used to capture the shapes of the produced preforms and the consolidated components. The preforms were scanned in-situ on the DDF machine whilst maintaining the vacuum consolidation pressure. Ambersil Flaw Detector was uniformly sprayed onto the surface of the outer diaphragm to avoid excessive reflection during scanning. Reference points were marked on the diaphragm using a red marker pen before scanning to assist with the alignment and stitching of individual scans taken at different angles, in order to create a full 3D representation of the preform. Due to the applied in-bag vacuum, it was assumed that there was no clearance between the top diaphragm and the uppermost fabric ply. The same scanning method was applied to the consolidated components and the

tool surface. Open-source software, CloudCompare [32], was used to visualise the distribution of defects by performing post-scan measurements on the point cloud.

3. Simulation approach

3.1. Material models

Each fabric ply was modelled using a composite layup based on the fabric material model developed by Yu et al. [30,38], comprising three artificial layers using laminate shell elements (S4R) within Abaqus/Explicit. A single integration point was assigned to the central layer to decouple the fabric bending stiffness from the in-plane stiffness. Element curvature in each fibre direction was updated based on strains at the integration points through the thickness of the shell element, enabling a non-linear bending stiffness-curvature relation to be incorporated into the forming simulation. A well-established non-orthogonal constitutive relation for biaxial fabrics [9,33,34] was employed to track the fibre directions as the fabric sheared in-plane. This enabled the bending contribution in each fibre direction to be taken into consideration, in order to update the fabric bending behaviour in relation to the shear deformation.

The mechanical behaviour of the diaphragm was modelled using the Marlow model for hyperelastic materials in Abaqus/Explicit [35]. The uniaxial stress-strain data in Table 2 was used to derive the mechanical responses for the other two deformation modes (i.e. equibiaxial tension and planar shear).

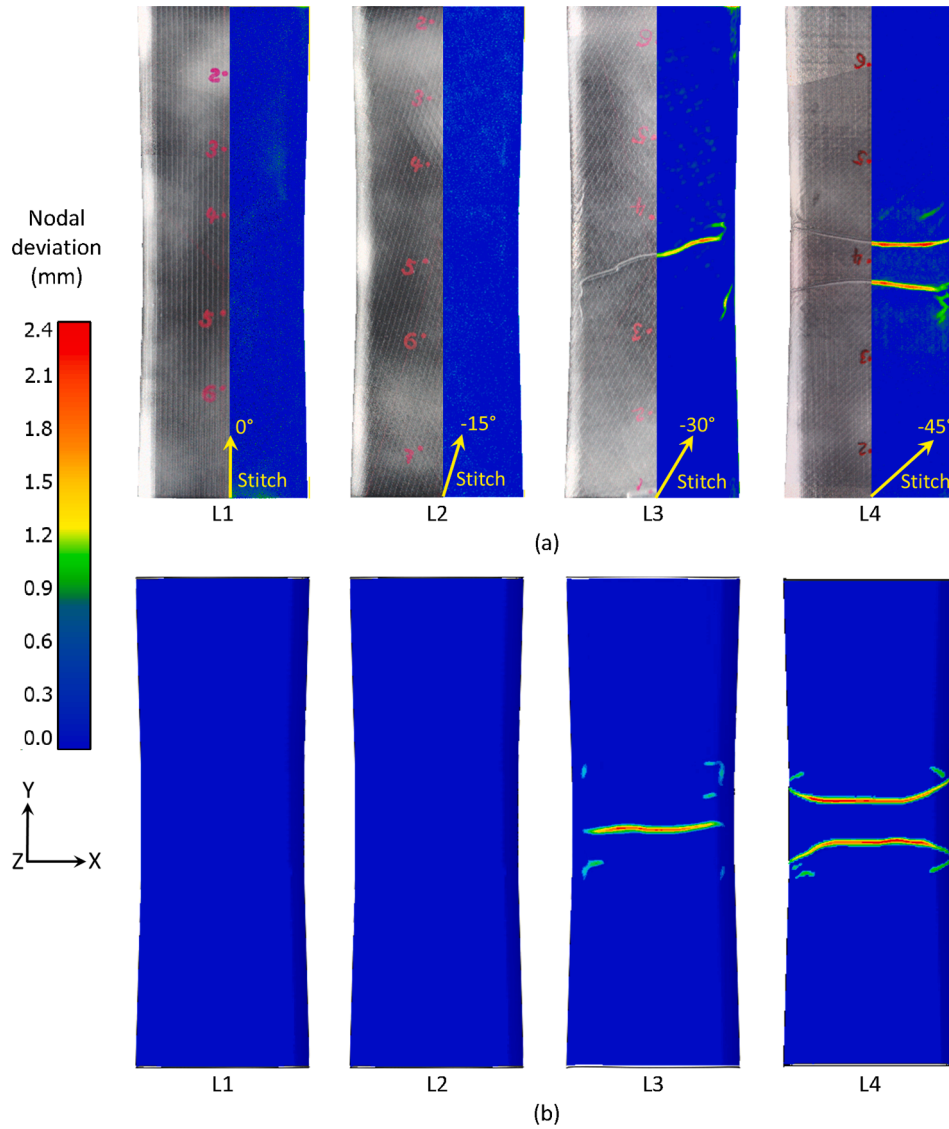


Fig. 6. Experimental and simulation results for the forming cases L1-L4 in Table 4. (a) Experimental scans (b) Numerical simulations.

3.2. DDF process model

The FE mesh representing the fabric plies was positioned between the mesh for the two diaphragms, as shown in Fig. 3(b). The in-bag vacuum between the two diaphragms was modelled using two pressures, which were equal in magnitude (1×10^5 Pa) but opposite in direction between times A and B in Fig. 3(b). The material assembly was draped over the tool until the edge of the lower diaphragm made contact with the machine bed, by applying displacement boundary conditions to the frame. The pressure between the bottom diaphragm and the machine bed was then reduced to zero, which generated a pressure gradient (from time B to C in Fig. 3(b)) to draw the diaphragm assembly into contact with the tool surface. All parts of the tooling were modelled as rigid bodies. Interactions between them were modelled using the in-built Abaqus penalty contact algorithm with Coulomb friction. Average CoF values were assigned for fabric-fabric and fabric-diaphragm pairings in

the FE model, as presented in Fig. 2. All CoF values used in the forming simulations are listed in Table 3, where $C_{fab-fab}^{fric}$, $C_{fab-dia}^{fric}$, $C_{dia-dia}^{fric}$ and $C_{dia-tool}^{fric}$ denote the coefficients for the fabric-fabric, fabric-diaphragm, diaphragm-diaphragm and diaphragm-tool interfaces respectively.

3.3. Wrinkle characterisation

The tool used in this study for the demonstrator component only has a moderate variation in surface curvature, therefore poor fabric-tool conformity related to fabric bridging was considered to be negligible. Out-of-plane fabric wrinkles were the only form of defect observed in this case and the nodal distance between the mesh of the uppermost fabric ply and the tool surface was used to quantify this. The total length of all wrinkles was calculated based on the simulation results to quantitatively assess wrinkling severity for each scenario.

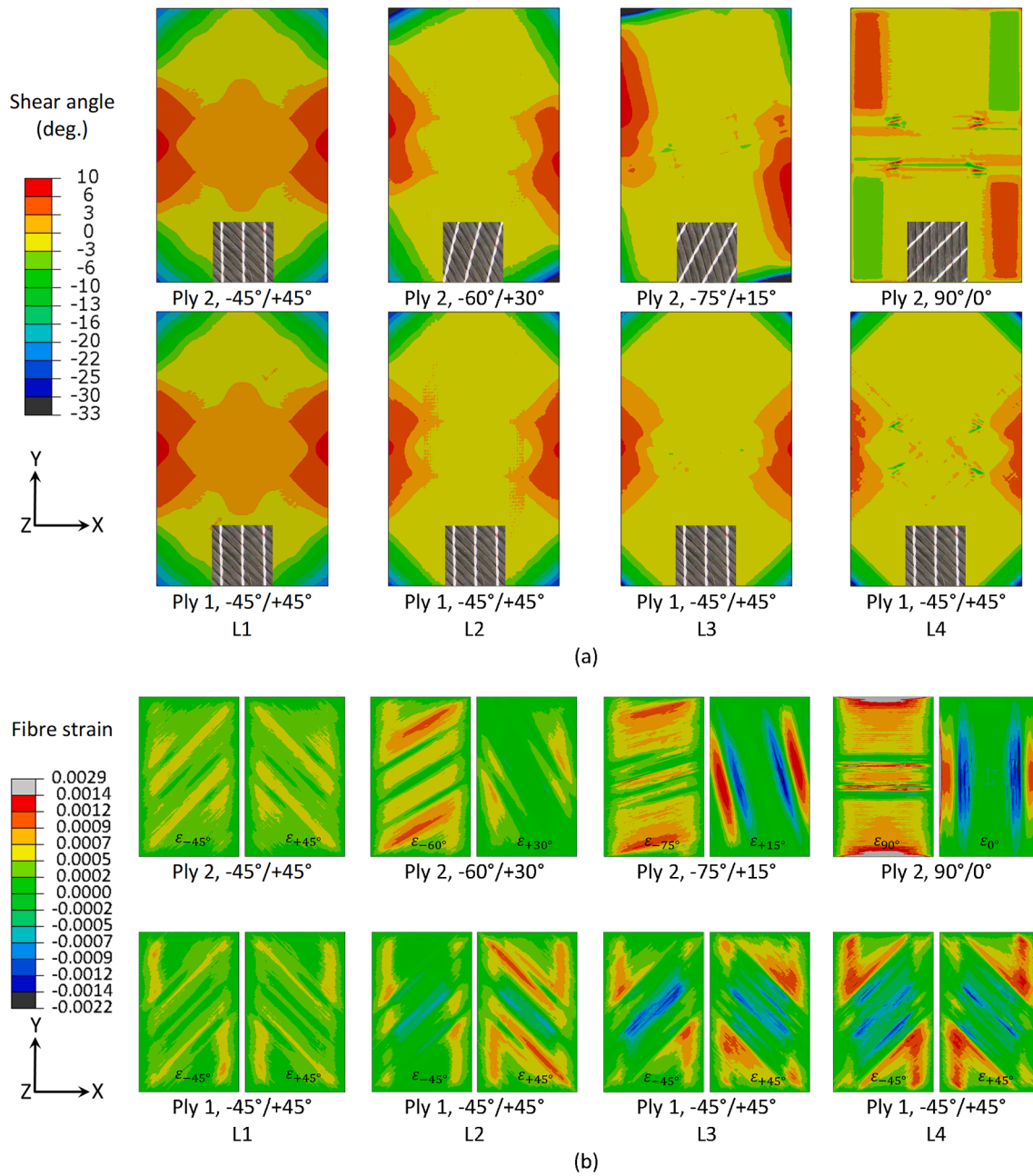


Fig. 7. Numerical predictions for the forming cases L1-L4 in Table 4. (a) Shear angle and (b) Fibre strain.

4. Results and discussion

4.1. Wrinkling mechanism in multi-ply forming

The results from the single ply cases (i.e. M1 and M2 in Table 4) are shown in Fig. 4, indicating no visible wrinkles on the surface of the preform. This confirms that the current tool geometry has a negligible effect on the formation of wrinkles for the individual ply orientations, therefore any wrinkles experienced for the multi-ply preforms can be attributed to relative inter-ply movement.

DDF simulations were also performed for a series of multi-ply layouts comprising two NCF plies to investigate the influence of ply orientation on the severity of wrinkling defects. As shown in Fig. 5(a), the stitch directions for the two NCF plies were initially aligned along the longitudinal direction of the tool (Y axis direction in Fig. 5(a)). The stitch direction of the uppermost ply was rotated clockwise in the X-Y plane, at an angular increment of 5° , producing a range of relative fibre angles at the contact interface between the two plies of 90° through to 0° . The nodal distance between the deformed mesh of the uppermost fabric ply and the tool surface was calculated to visualise the surface defects.

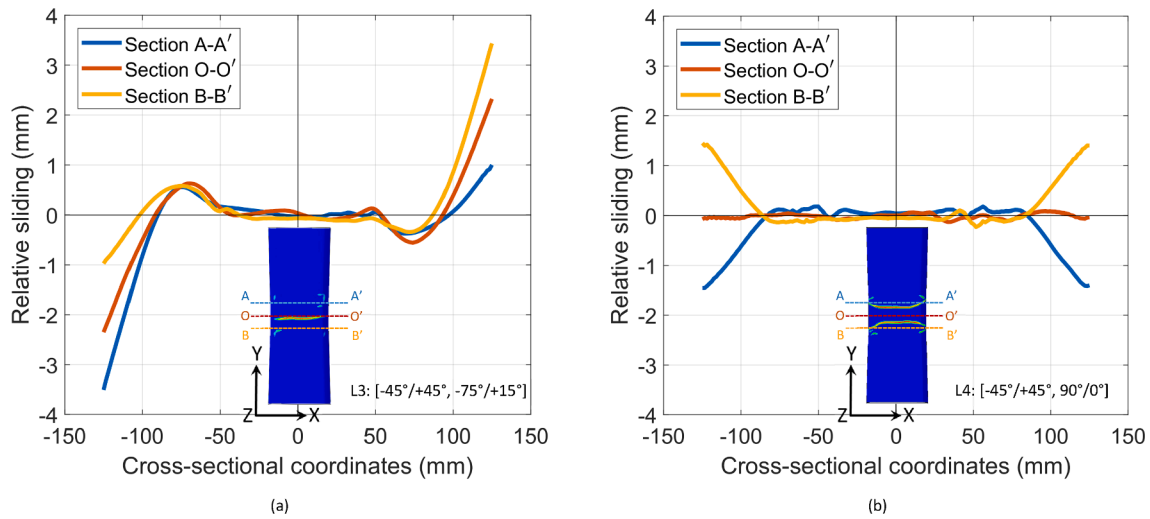


Fig. 8. Relative sliding displacement of the upper ply with respect to the lower ply for the layups (a) L3 and (b) L4 in the longitudinal direction of the tool (Y-axis). Section O-O' is taken from the middle of the specimen and sections A-A' and B-B' are taken at 30 mm spacings from the middle section O-O'.

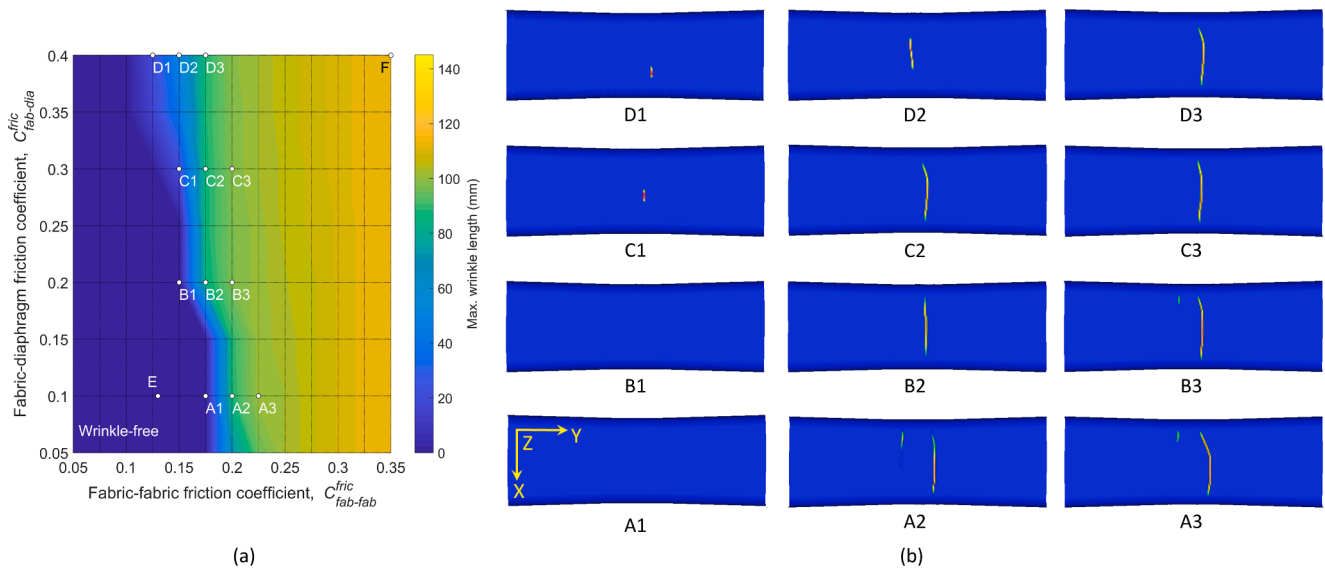


Fig. 9. (a) Contour map of the maximum wrinkle length predicted by the FE model using different friction coefficients for the ply layout L3 [-45°/+45°, -75°/+15°] (b) Typical wrinkle patterns corresponding to the data points on the contour plot.

The total wrinkle lengths (sum of the length of all wrinkles with an amplitude greater than 1 mm) for all layups are plotted in Fig. 5(a), along with the corresponding wrinkle patterns in Fig. 5(b). Wrinkling occurs in all preforms with relative fibre angles at the interface ranging from 20° to 70°. The total wrinkle length peaks at a value of 401 mm when the relative fibre angle reaches 45°. The distribution is symmetrical about this point and the total wrinkle length is reduced as the relative fibre angle tends to 0° or 90°. The relative fibre orientation at the contact interface is demonstrated to have a significant influence on both the severity of wrinkles and the pattern, particularly since the friction coefficient used for all ply-ply combinations was identical. A relative fibre angle of 45° at the ply interface is most likely to induce wrinkles in the preform, especially when the geometry of the formed shape causes relative displacement between the plies. Similar findings

have been reported in the literature [16,19] during the forming of multi-layered UD preforms.

The wrinkling patterns for layups L1 – L4 (see Table 4 for layup sequences) produced by the forming simulation are compared with the experimental results in Fig. 6 to validate the FE model. There is good agreement between the simulations and experiments for layups L1 and L2, where no wrinkles are found in the preform. For layup L4, two wrinkles with similar length (~138 mm on average) occur in the middle recessed region of the preform, which is close to the wrinkle pattern and length (~142 mm on average) predicted by the FE model. A primary wrinkle length of 113 mm is generated in the middle of the L3 experimental layup, compared with 109 mm in the FE simulation, but the orientation of the main wrinkle differs to that from the experimental result. In addition, some minor wrinkles also occurred around the fillet

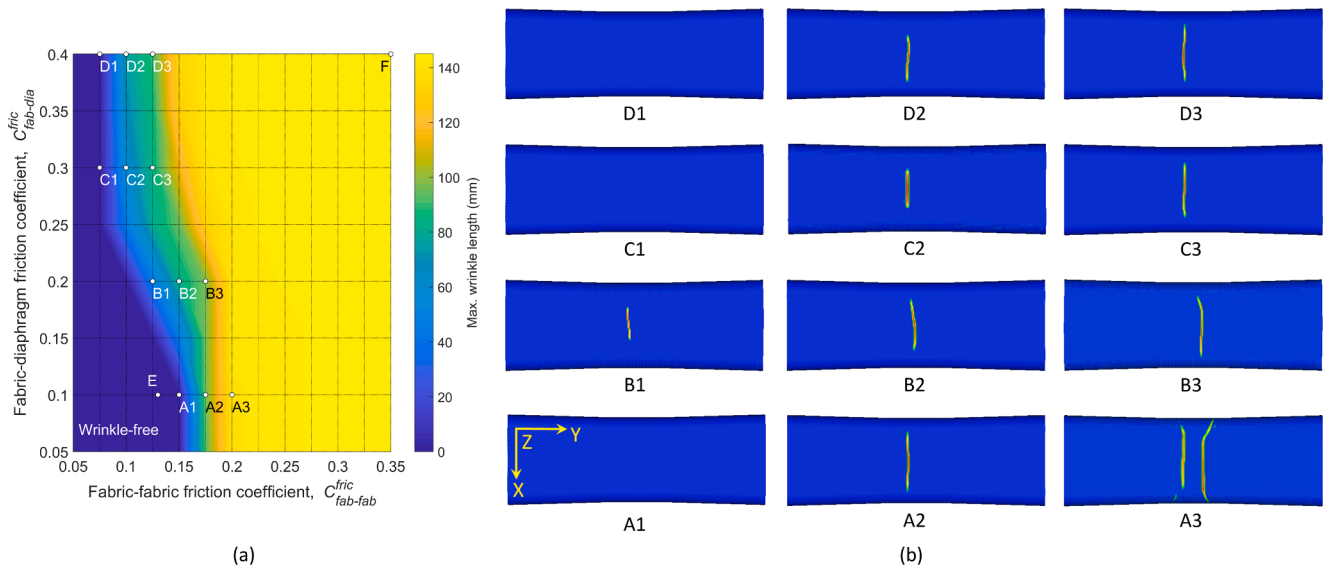


Fig. 10. (a) Contour map of the maximum wrinkle length predicted by the FE model using different friction coefficients for the layup L4 [-45°/+45°, 90°/0°] and (b) Typical wrinkle patterns corresponding to the data points (i.e. black dots) in (a) on the contour plot.

edges of the tool, which are captured by the FE model.

Fig. 7(a) shows the shear angle distributions overlaid onto the undeformed blank for the four layups, (L1 – L4 in Table 4). Since the tool exhibits gentle ramp ratios on all surfaces (see Fig. 3), the bridging effects related to the recess area of the tool are insignificant. As a result, the positive shear deformation required for the fabric plies to conform to the tool surface in the ramp area is relatively small in magnitude ($<10^\circ$) for all layup configurations. However, Fig. 7(a) demonstrates that the layups comprising two plies of different fibre orientations (L2, L3 and L4) undergo different shear deformations during forming, with a tendency to produce inter-ply movements. This is restricted by the frictional resistance at the ply-ply contact interfaces, causing local compression along the fibre directions, as shown in Fig. 7(b). Consequently, this local compressive strain causes the fibres to buckle and therefore wrinkle in the corresponding areas. The magnitude of the compressive strain increases as the relative fibre angle at the interface decreases from 90° to 45° for the four layups presented, highlighting the dependency of fabric wrinkling on the layup sequence. The likelihood of inter-ply sliding is dominated by the layup sequence for the current geometry, with the interfacial frictional force activated only when relative inter-ply sliding occurs. The effect of the interfacial CoF on the severity of wrinkling is studied in more detail in Section 4.2.

Based on the changes in nodal coordinates of the deformed mesh, the relative displacement along the longitudinal direction of the tool (Y-axis in Fig. 8) was calculated at three cross-sections in the central recess region of the specimen (i.e. Sections A-A', O-O' and B-B' in Fig. 8) for layups L3 and L4, as shown in Fig. 8. Section O-O' is at the geometric centre of the specimen, and the vertical distance from Section O-O' to A-A' and B-B' is 30 mm in each case. The relative sliding at the three cross-sections for layup L4 ($[-45^\circ/+45^\circ, 90^\circ/0^\circ]$) are presented in Fig. 8(b). All three sections exhibit symmetrical sliding about the longitudinal direction of the tool, resulting in a symmetrical wrinkle pattern. For layup L3 ($[-45^\circ/+45^\circ, -75^\circ/+15^\circ]$), the relative sliding displacements at all three cross-sections are asymmetric about the length of the specimen (see Fig. 8(a)), indicating a counter-clockwise rotation of the upper

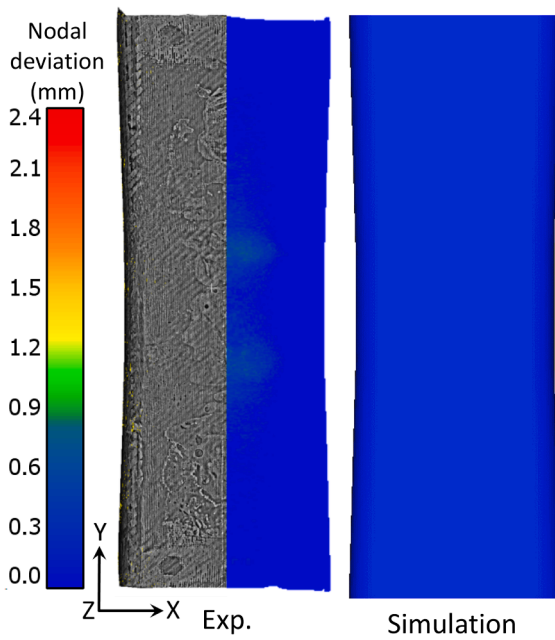
ply with respect to the lower ply. This relative rotation is restricted by the resistance from the inter-ply friction, leading to an oblique wrinkle across the middle of the specimen. Furthermore, the frictional force caused by this asymmetric inter-ply motion is dependent on the fibre orientation and the stitch pattern at the contact interface, both of which influence the size and shape of the asperities at the contact surface and therefore the CoF. The orientation dependence of the CoF has not been studied in detail in the current work, therefore a constant value has been assumed, which may contribute to the error in the prediction of the wrinkle orientation for layup L3 in Fig. 6. An isotropic Coulomb friction model has been employed, but an anisotropic model maybe required to account for this orientation dependence.

4.2. Influence of interfacial friction

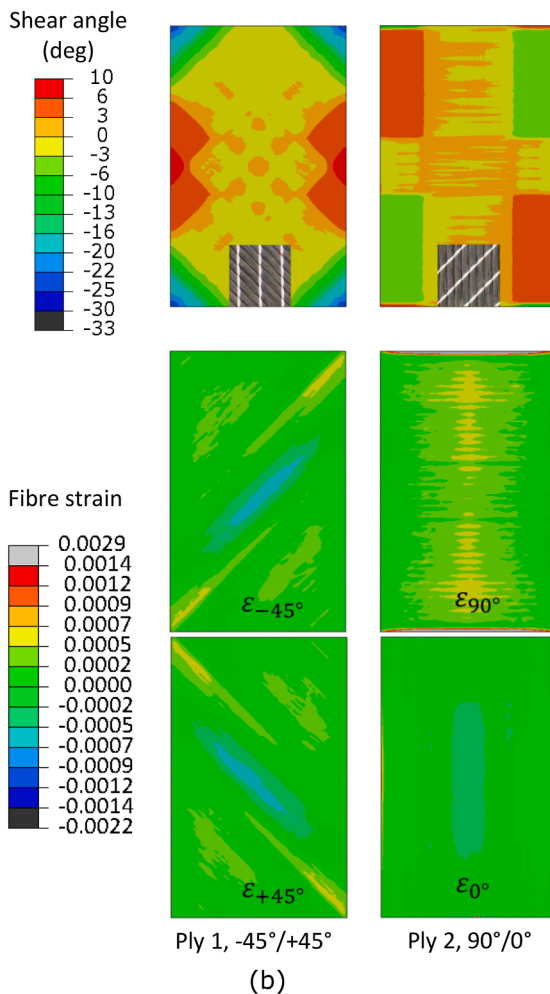
A parametric study was performed using DDF simulations with different combinations of fabric-fabric and fabric-diaphragm CoF to evaluate the influence of friction on the formation of fabric wrinkles. Layups L3 and L4 (Table 4) were selected for this study, where the fabric-fabric CoF was varied from 0.05 to 0.35 in increments of 0.025 and the fabric-diaphragm CoF was varied from 0.05 to 0.4 in increments of 0.05.

Contour plots for the maximum wrinkle length, using different CoF combinations, are shown in Fig. 9(a) and Fig. 10(a) for layups L3 and L4 respectively. These maps were created by interpolating the discrete data points at the grid intersections, which denote different combinations of the friction coefficients. The corresponding wrinkle patterns are plotted for L3 and L4 at the data points near the boundary between the wrinkle-free and the wrinkled region in the maps, as shown in Fig. 9(b) and Fig. 10(b) respectively.

On average, the severity of wrinkles, represented by the maximum wrinkle length (Fig. 9(b) and Fig. 10(b)), increases with the increase in both $C_{fab-fab}^{fric}$ and $C_{fab-dia}^{fric}$ friction coefficients. The preform is free of wrinkles for the entire range of $C_{fab-dia}^{fric}$ (i.e. $0.05 \leq C_{fab-fab}^{fric} \leq 0.4$) when $C_{fab-fab}^{fric}$ is small. For layup L3, $C_{fab-fab}^{fric}$ must be less than or equal to 0.125,



(a)



(b)

Fig. 11. (a) Surface scan of the consolidated layup L4 [-45°/+45°, 90°/0°]. (b) Shear angle and fibre strains of individual plies within the layup predicted using the reduced inter-ply friction coefficients listed in Table 4.

and for L4 $C_{fab-fab}^{fric}$ must be less than or equal to 0.075. As $C_{fab-fab}^{fric}$ increases, wrinkles are inevitable for all values of $C_{fab-dia}^{fric}$ when $C_{fab-fab}^{fric}$ exceeds 0.20 for L3 and 0.175 for L4. This indicates that the occurrence of wrinkles is more sensitive to the fabric-fabric friction resistance than the fabric-diaphragm friction resistance in this case. As shown in Fig. 9 (a) and Fig. 10(a), the area of the wrinkle-free region (dark blue) for L4 [-45°/+45°, 90°/0°] is smaller than the one for L3 [-45°/+45°, -75°/+15°], which suggests that the layup with a relative fibre angle of 45° at the ply interface is more likely to induce wrinkles. The influence of $C_{fab-fab}^{fric}$ is likely to become more dominant as the number of plies and therefore ply interfaces increases within the layup.

A qualitative assessment of fibre lubrication was conducted experimentally to understand the influence of the reduced inter-ply CoF on the wrinkle pattern. Friction coefficients $C_{fab-fab}^{fric}$ and $C_{fab-dia}^{fric}$ were measured following liquid resin lubrication, as listed in Table 3. The corresponding combinations ($C_{fab-fab}^{fric}$, $C_{fab-dia}^{fric}$) are represented by Point E in Fig. 9(a) and Fig. 10(a), which falls in the wrinkle-free regions for both L3 and L4. Comparing the dry (non-lubricated) friction case for each layup (Point F) with the resin lubricated friction case (Point E), demonstrates that local resin lubrication could be a potential solution for mitigating wrinkles caused by interfacial interaction during multi-ply fabric forming.

4.3. Wrinkle mitigation validation

Layups L4 and L5 were experimentally formed (see Table 4) to validate the concept of applying the liquid resin as an inter-ply lubricant for wrinkle mitigation. L4 consists of two biaxial NCF plies, i.e. [-45°/+45°, 90°/0°], while the layup in case L5 is more generic, comprising four biaxial NCF plies laid up in a balanced symmetric sequence [0°/90°, +45°/-45°, -45°/+45°, 90°/0°].

Fig. 11(a) shows a 3D scan of the uppermost surface of the consolidated part produced using layup L4 (i.e. [-45°/+45°, 90°/0°]), compared with the corresponding simulation result. The deviation distance is calculated by comparing the surface of the component against the tool surface, with the average thickness of the component deducted from the deviation distance to visualise any potential wrinkling defects. Results show that out-of-plane wrinkling has been successfully eliminated compared to the experimental scan for the same layup without liquid resin lubrication (see L4 in Fig. 6(a)). A DDF simulation was performed using the friction coefficients measured with lubrication (see Table 4). As shown in Fig. 11(b), the distribution of the predicted shear angles in each ply is similar to those predicted for the same layup in Fig. 7(a) without lubrication. However in contrast, the compressive strains in the fibre directions are alleviated by the lubrication effect, compared to the results for L4 without lubrication in Fig. 7(b), due to the reduction in the interfacial friction.

For the balanced symmetric layup L5 (i.e. [0°/90°, +45°/-45°, -45°/+45°, 90°/0°]), two curved wrinkles are observed near the central ramp area of the tool, which are similar in shape to those from the FE prediction, as shown in Fig. 12(a). In the experiment, the two primary wrinkles are initiated at the edge fillet as the ply stack bends. As shown in Fig. 12(b), Ply 1 and Ply 2 undergo very different shear deformations, which generates dissimilar slippage between fibres at the contact interface. This is also observed at the interface between Ply 3 and Ply 4. The predicted shear angles of the inner plies (Ply 2 and Ply 3) are similarly distributed but are opposite in sign. This indicates that the yarns in the contact pairing between Ply 2 and Ply 3 rotate in the same direction at each point in the contact region, as shown in the schematic in Fig. 13. Thus, the relative movement of the yarns at the contact interface between Ply 2 and Ply 3 is negligible. Consequently, the compressive strains along the fibre directions in Fig. 12(b) are caused by relative yarn rotation at the interfaces between Ply 1 and Ply 2 and between Ply 3 and Ply 4, where the relative fibre angle at both interfaces is 45°.

The prediction from the FE simulation for L5 produces a wrinkle

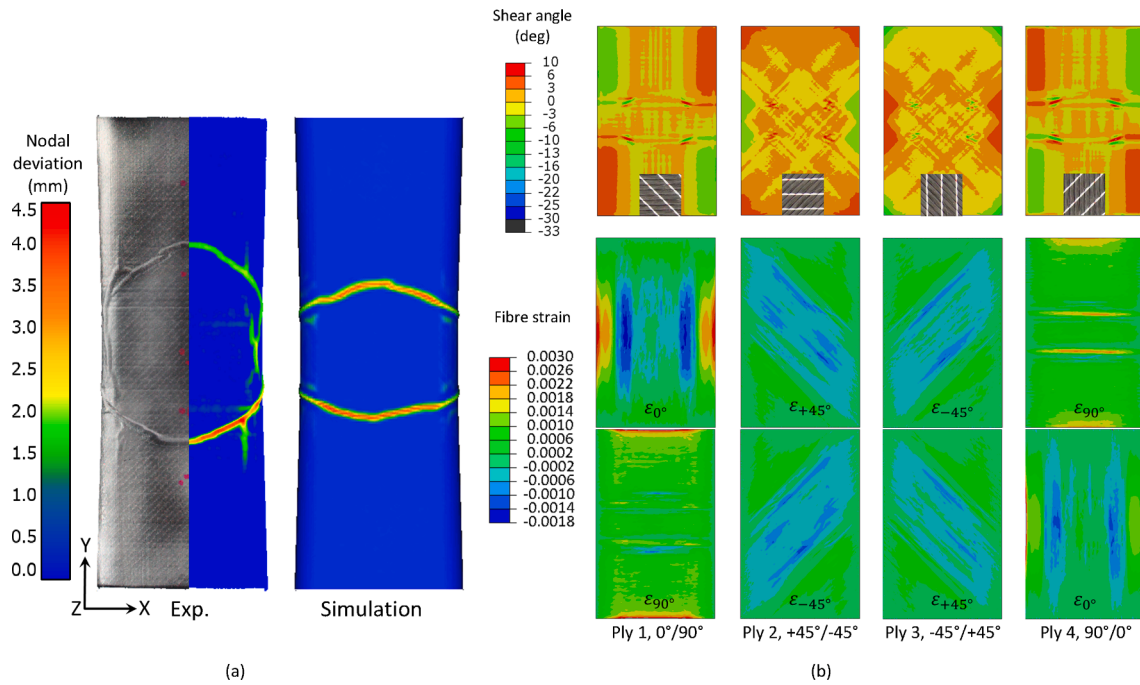


Fig. 12. (a) Comparison of wrinkle patterns obtained from experiment and simulation for the layup L5 (i.e. $[0^\circ/90^\circ, +45^\circ/-45^\circ]$ s) without lubrication. (b) Shear angle and fibre strains predicted by the FE model using friction coefficients of dry material interfaces listed in Table 4.

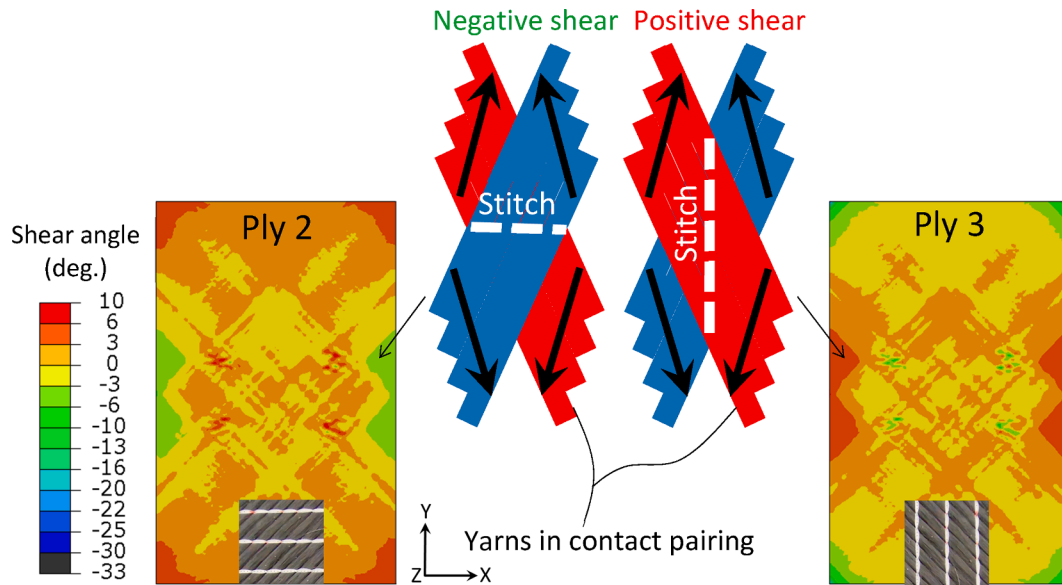


Fig. 13. Schematic of yarn rotation for a local contact region at the interface between Ply 2 and Ply 3 in Fig. 12(b).

pattern similar in shape, but the peak distance between the wrinkles is smaller in the longitudinal direction of the tool (Fig. 12(a)). When the thickness of the fabric layup is considerably larger than that of the diaphragms, the fabric-fabric interaction becomes one of the dominant factors in defect formation during multi-ply forming. This reinforces the

need for an anisotropic friction model to capture the complex inter-ply behaviour. The CoF is dependent on the normal force applied during compaction, which will therefore be influenced by local variations in the through-thickness compaction pressure produced by the in-bag vacuum. This compaction may also influence the bending and shear stiffness of

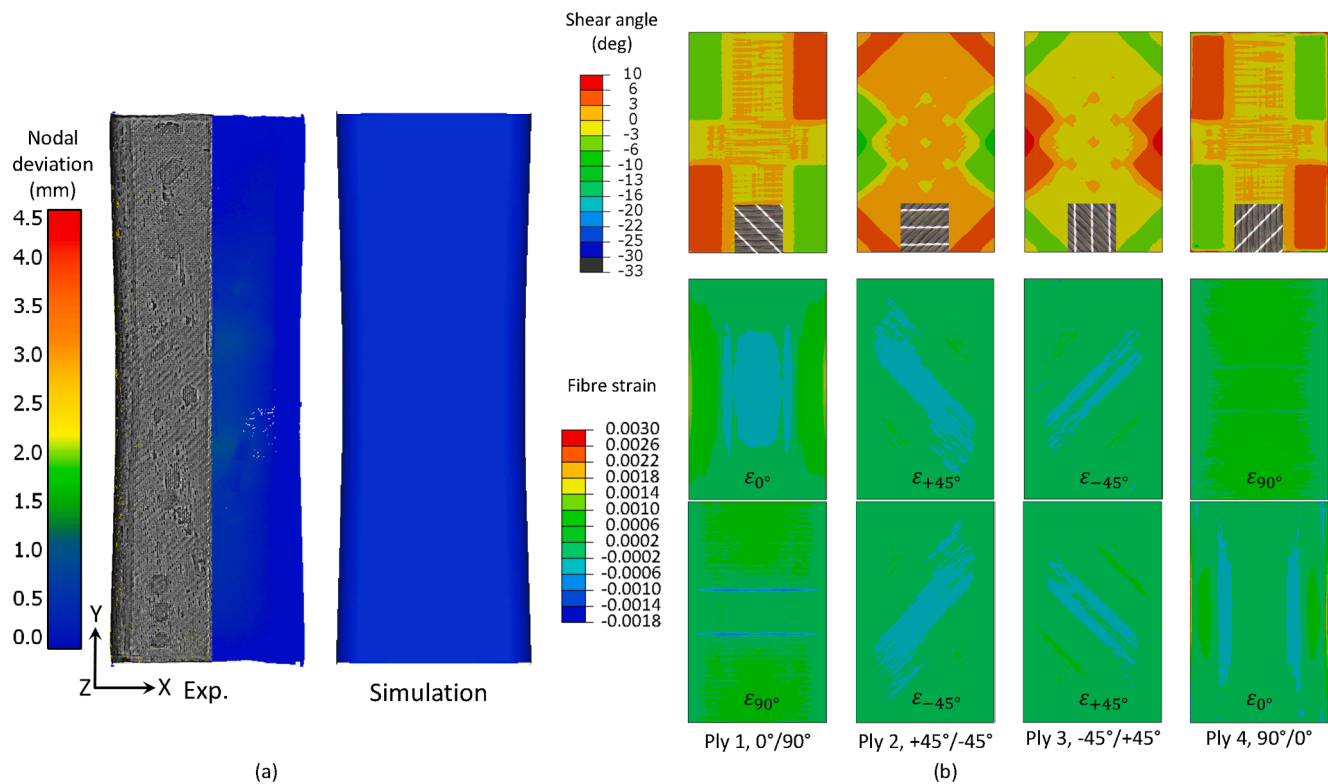


Fig. 14. (a) Surface scan and nodal deviation distance of the consolidated layout L5 [0°/90°, +45°/-45°]s. (b) Shear angle and fibre strains of individual plies within the layout predicted using the reduced inter-ply friction coefficients listed in Table 4.

the fabric plies by increasing the inter-fibre friction [36,37]. The material behaviour may need to be characterised in-situ within the diaphragms to take into account the effect of the vacuum pressure [38].

Liquid resin was also used as a lubrication for layout L5 (see Table 4) and no wrinkles were observed on the corresponding consolidated component, as shown in Fig. 14(a). According to the simulation results, the fibre compressive strain (Fig. 14(b)) has been significantly reduced by approximately 70% compared to the case without lubrication (see Fig. 12(b)). This highlights the importance of reducing interfacial friction to mitigate wrinkles during multi-ply NCF forming.

5. Conclusions

Multi-ply NCF forming behaviour in DDF has been investigated via experiments and numerical simulation. Simulation results show that dissimilar shear deformation between adjacent plies can cause relative sliding at the contact interface, leading to compressive stresses in fibres and consequently out-of-plane wrinkling. The predicted wrinkle pattern generally agreed well with experimental observations. The orientation of wrinkles can be affected by the direction of inter-ply sliding, which implies that a more sophisticated friction model is required to take into consideration the influence of the fibre orientation and stitch pattern at the contact interface for multi-ply forming simulations.

A relative fibre angle of 45° at the ply interface was found to be undesirable in terms of the overall formed quality of multi-ply NCF preforms. A parametric study was performed to establish if the quality of

the formed shape could be improved for layouts containing relative fibre angles of 45° for adjacent plies, by controlling the CoF at the inter-ply interface. Results indicate that the severity of wrinkles is strongly affected by the fabric-fabric friction resistance between the NCF plies, whereas the fabric-diaphragm friction appears to be less significant.

Experimental friction tests showed that fabric lubrication using liquid resin can result in a reduction in frictional force by over 64% for the NCF and diaphragm materials used. Liquid resin was applied to fabric-fabric and fabric-diaphragm contact interfaces, which successfully mitigated wrinkles during multi-ply NCF forming of quad-axial layouts using the current geometry. This indicates that reducing inter-ply friction is an effective approach to eliminating macroscale wrinkles induced by excessive inter-ply sliding.

CRediT authorship contribution statement

F. Yu: Conceptualisation, Methodology, Validation, Writing – original draft. **S. Chen:** Methodology, Writing – original draft. **L.T. Harper:** Supervision, Funding acquisition, Writing – review & editing. **N.A. Warrior:** Supervision, Writing – review & editing.

Declaration of Competing Interest

The authors declare that they have no known competing financial interests or personal relationships that could have appeared to influence

the work reported in this paper.

Acknowledgements

This work was partially funded by the Engineering and Physical Sciences Research Council, as part of the “EPSRC Future Composites Manufacturing Research Hub” (EP/P006701/1). The authors would also like to acknowledge funding from the China Scholarship Council (CSC) and the Aviation Industry Corporation of China (AVIC).

Appendix A:. Friction behaviour characterisation by sled test

The fabric-fabric frictional behaviour was characterised using the sled test (see Fig. 1) for six combinations of relative fibre orientations at the contact interface, as shown in Fig. A1. Similarly, the fabric-diaphragm friction forces were measured for three different fibre orientations with respect to the sliding direction as shown in Fig. A2. Curves were also produced for the diaphragm-diaphragm contact pairing, with and without liquid resin lubrication (see Fig. A3). The pulling force versus sliding displacement curves in Figs. A1 to A3 represent the mean values calculated from five test repeats, with the error bars representing the standard deviation at each data point.

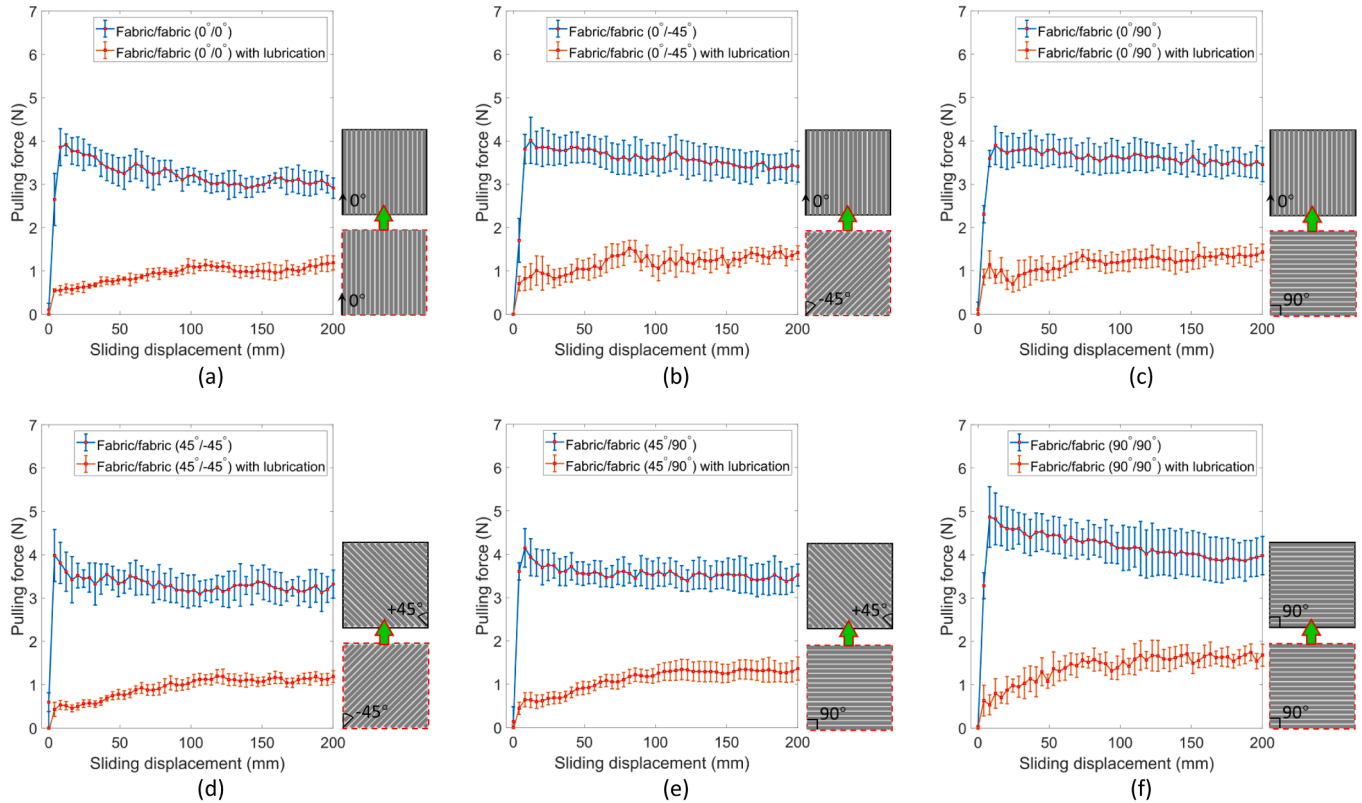


Fig. A1. Pulling force vs. sliding displacement curves for fabric-fabric interfaces corresponding to different ply-ply relative orientations, measured with and without liquid resin lubrication. Error bars denote the standard deviation from 5 experimental repeats.

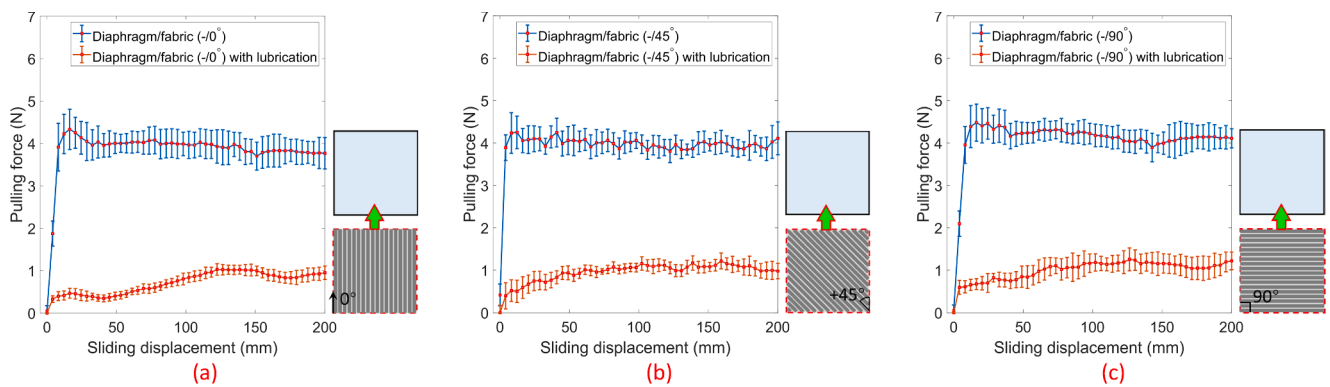


Fig. A2. Pulling force vs. sliding displacement curves for fabric-diaphragm interfaces corresponding to different ply-ply relative orientations, measured with and without liquid resin lubrication. Error bars denote the standard deviation from 5 experimental repeats.

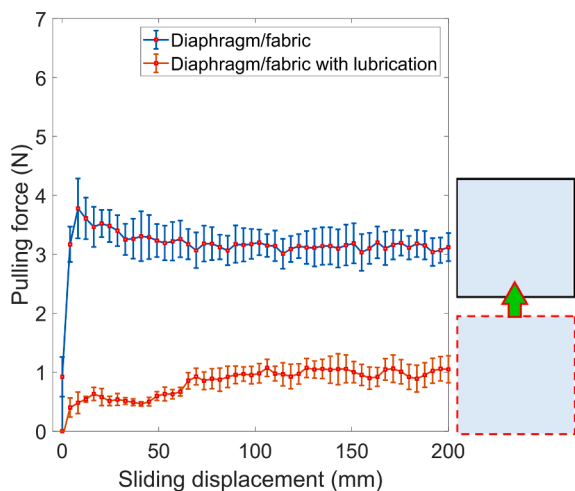


Fig. A3. Pulling force vs. sliding displacement curves for diaphragm-diaphragm interfaces, measured with and without liquid resin lubrication. The error bars denote the standard deviation from 5 experimental repeats.

References

- Allaoui S, Cellard C, Hivet G. Effect of inter-ply sliding on the quality of multilayer interlock dry fabric preforms. *Compos A Appl Sci Manuf* 2015;68:336–45. <https://doi.org/10.1016/j.compositesa.2014.10.017>.
- Nosrat Nezami F, Gereke T, Cherif C. Analyses of interaction mechanisms during forming of multilayer carbon woven fabrics for composite applications. *Compos A Appl Sci Manuf* 2016;84:406–16. <https://doi.org/10.1016/j.compositesa.2016.02.023>.
- Guzman-Maldonado E, Wang P, Hamila N, Boisse P. Experimental and numerical analysis of wrinkling during forming of multi-layered textile composites. *Compos Struct* 2019;208:213–23. <https://doi.org/10.1016/j.compstruct.2018.10.018>.
- Mukhopadhyay S, Jones MI, Hallett SR. Tensile failure of laminates containing an embedded wrinkle; numerical and experimental study. *Compos A Appl Sci Manuf* 2015;77:219–28. <https://doi.org/10.1016/j.compositesa.2015.07.007>.
- Mukhopadhyay S, Jones MI, Hallett SR. Compressive failure of laminates containing an embedded wrinkle; experimental and numerical study. *Compos A Appl Sci Manuf* 2015;73:132–42. <https://doi.org/10.1016/j.compositesa.2015.03.012>.
- Lightfoot JS, Wisnom MR, Potter K. Defects in woven preforms: Formation mechanisms and the effects of laminate design and layup protocol. *Compos A* 2013; 51:99–107. <https://doi.org/10.1016/j.compositesa.2013.04.004>.
- Xie N, Smith RA, Mukhopadhyay S, Hallett SR. A numerical study on the influence of composite wrinkle defect geometry on compressive strength. *Mater Des* 2018; 140:7–20. <https://doi.org/10.1016/j.matdes.2017.11.034>.
- Dumont F, and C. Weimer, 19 - Non-crimp fabric: preforming analysis for helicopter applications, in *Non-Crimp Fabric Composites*, S.V. Lomov, Editor. 2011, Woodhead Publishing. p. 449–460.
- Chen S, McGregor OPL, Harper LT, Endruweit A, Warrior NA. Defect formation during preforming of a bi-axial non-crimp fabric with a pillar stitch pattern. *Compos A Appl Sci Manuf* 2016;91:156–67. <https://doi.org/10.1016/j.compositesa.2016.09.016>.
- Wang L, Wang J, Liu M, Peng X. Development and verification of a finite element model for double diaphragm preforming of unidirectional carbon fiber prepreg. *Compos A Appl Sci Manuf* 2020;135:105924. <https://doi.org/10.1016/j.compositesa.2020.105924>.
- Dodwell TJ, Butler R, Hunt GW. Out-of-plane ply wrinkling defects during consolidation over an external radius. *Compos Sci Technol* 2014;105:151–9. <https://doi.org/10.1016/j.compscitech.2014.10.007>.
- Farnand K, Zobeiry N, Poursartip A, Fernlund G. Micro-level mechanisms of fiber waviness and wrinkling during hot drape forming of unidirectional prepreg composites. *Compos A Appl Sci Manuf* 2017;103:168–77. <https://doi.org/10.1016/j.compositesa.2017.10.008>.
- Hallander P, Åkermo M, Mattei C, Petersson M, Nyman T. An experimental study of mechanisms behind wrinkle development during forming of composite laminates. *Compos A Appl Sci Manuf* 2013;50:54–64. <https://doi.org/10.1016/j.compositesa.2013.03.013>.
- Leutz D, Vermilyea M, Bel S, Hinterhölzl R. Forming Simulation of Thick AFP Laminates and Comparison with Live CT Imaging. *Appl Compos Mater* 2016;23(4): 583–600. <https://doi.org/10.1007/s10443-016-9475-6>.
- Hallander P, Sjölander J, Åkermo M. Forming induced wrinkling of composite laminates with mixed ply material properties; an experimental study. *Compos A Appl Sci Manuf* 2015;78:234–45. <https://doi.org/10.1016/j.compositesa.2015.08.025>.
- Sjölander J, Hallander P, Åkermo M. Forming induced wrinkling of composite laminates: A numerical study on wrinkling mechanisms. *Compos A Appl Sci Manuf* 2016;81:41–51. <https://doi.org/10.1016/j.compositesa.2015.10.012>.
- Alshahrani H, Hoggati M. Experimental and numerical investigations on formability of out-of-autoclave thermoset prepreg using a double diaphragm process. *Compos A Appl Sci Manuf* 2017;101:199–214. <https://doi.org/10.1016/j.compositesa.2017.06.021>.
- ten Thije RHW, Akkerman R. A multi-layer triangular membrane finite element for the forming simulation of laminated composites. *Compos A Appl Sci Manuf* 2009; 40(6–7):739–53. <https://doi.org/10.1016/j.compositesa.2009.03.004>.
- Johnson KJ, Butler R, Loukaides EG, Scarth C, Rhead AT. Stacking sequence selection for defect-free forming of uni-directional ply laminates. *Compos Sci Technol* 2019;171:34–43. <https://doi.org/10.1016/j.compscitech.2018.11.048>.
- Åkermo M, Larberg Y, Sjölander J, Hallander P. Influence of interply friction on the forming of stacked prepreg. In: *The 19th International Conference on Composite Materials (ICCM19)*, July 28 to August 2, 2013 in Montreal, Canada. Inc: Curran Associates; 2013. p. 919–28.
- Zhao Y, Zhang T, Li H, Zhang B. Characterization of prepreg-prepreg and prepreg-tool friction for unidirectional carbon fiber/epoxy prepreg during hot diaphragm forming process. *Polym Test* 2020;84:106440. <https://doi.org/10.1016/j.polymertesting.2020.106440>.
- Alshahrani, H. and M. Hoggati, Optimum processing parameters for hot drape forming of out-of-autoclave prepreg over complex shape using a double diaphragm technique, in *20th International Conference on Composite Materials*. 2015: Copenhagen.
- Sun J, Gu Y, Li M, Ma X, Zhang Z. Effect of forming temperature on the quality of hot diaphragm formed C-shaped thermosetting composite laminates. *J Reinf Plast Compos* 2012;31(16):1074–87. <https://doi.org/10.1177/0731684412453778>.
- Larberg YR, Åkermo M. On the interply friction of different generations of carbon/epoxy prepreg systems. *Compos A Appl Sci Manuf* 2011;42(9):1067–74. <https://doi.org/10.1016/j.compositesa.2011.04.010>.
- Pasco C, Khan M, Gupta J, Kendall K. Experimental investigation on interply friction properties of thermoset prepreg systems. *J Compos Mater* 2018;53(2): 227–43. <https://doi.org/10.1177/0021998318781706>.
- Bian XX, Gu YZ, Sun J, Li M, Liu WP, Zhang ZG. Effects of Processing Parameters on the Forming Quality of C-Shaped Thermosetting Composite Laminates in Hot Diaphragm Forming Process. *Appl Compos Mater* 2013;20(5):927–45. <https://doi.org/10.1007/s10443-012-9310-7>.
- Wang W-T, Yu H, Potter K, Kim BC. Improvement of composite drape forming quality by enhancing interply slip. *European Society for Composite Materials*; 2016.
- Chen S, McGregor OPL, Harper LT, Endruweit A, Warrior NA. Optimisation of local in-plane constraining forces in double diaphragm forming. *Compos Struct* 2018; 201:570–81. <https://doi.org/10.1016/j.compstruct.2018.06.062>.
- Chen S, McGregor OPL, Endruweit A, Elsmore MT, De Focatiis DSA, Harper LT, et al. Double diaphragm forming simulation for complex composite structures. *Compos A Appl Sci Manuf* 2017;95:346–58. <https://doi.org/10.1016/j.compositesa.2017.01.017>.
- Yu F, Chen S, Viisainen JV, Sutcliffe MPF, Harper LT, Warrior NA. A macroscale finite element approach for simulating the bending behaviour of biaxial fabrics. *Compos Sci Technol* 2020;191. <https://doi.org/10.1016/j.compscitech.2020.108078>.
- Yu F, Chen S, Harper LT, Warrior NA. Double diaphragm forming simulation using a global-to-local modelling strategy for detailed defect detection in large structures. *Compos A Appl Sci Manuf* 2021;147:106457. <https://doi.org/10.1016/j.compositesa.2021.106457>.
- CloudCompare 2.11, Retrieved from, <http://www.cloudcompare.org>. Accessed.
- Khan MA, Mabrouki T, Vidal-Sallé E, Boisse P. Numerical and experimental analyses of woven composite reinforcement forming using a hypoelastic behaviour. Application to the double dome benchmark. *J Mater Process Technol* 2010;210(2): 378–88. <https://doi.org/10.1016/j.jmatprotec.2009.09.027>.
- Badel P, Gauthier S, Vidal-Sallé E, Boisse P. Rate constitutive equations for computational analyses of textile composite reinforcement mechanical behaviour during forming. *Compos A Appl Sci Manuf* 2009;40(8):997–1007. <https://doi.org/10.1016/j.compositesa.2008.04.015>.
- Marlow R. A general first-invariant hyperelastic constitutive model. *Constitutive Models for Rubber* 2003:157–60.
- Alshahrani H, Hoggati M. Influence of double-diaphragm vacuum compaction on deformation during forming of composite prepregs. *J Sci: Adv Mater Devices* 2016; 1(4):507–11. <https://doi.org/10.1016/j.jsamd.2016.09.003>.
- Liang B, Colmars J, Boisse P. A shell formulation for fibrous reinforcement forming simulations. *Compos A Appl Sci Manuf* 2017;100:81–96. <https://doi.org/10.1016/j.compositesa.2017.04.024>.
- Yu F, Chen S, Harper LT, Warrior NA. Double diaphragm forming simulation using a global-to-local modelling strategy for detailed defect detection in large structures. *Compos A Appl Sci Manuf* 2021;147:106–457. <https://doi.org/10.1016/j.compositesa.2021.106457>.